SAND2005-7523P

ODT: Stochastic Simulation of Multi-Scale Dynamics

Alan R. Kerstein

Combustion Research Facility
Sandia National Laboratories
Livermore, California 94551-0969
USA
arkerst@sandia.gov

1 A New Modeling Paradigm

1.1 Motivation

The historical roots of the current paradigm for numerical simulation of turbulent flows can be traced to early attempts at weather prediction. The mesh that is used is typically far too coarse to resolve all relevant processes, so subgrid parameterizations are introduced to represent unresolved processes and their coupling to the resolved flow.

This approach has been successful in many contexts, enabling useful predictions of the unresolved processes as well as the resolved flow. However, as computing power increases and expectations of model performance increase commensurately, it is not self-evident that this paradigm will continue to be the optimal choice for all cases of interest. A particular challenge that is emphasized here is turbulent flow coupled to multiple physical and chemical processes at small scales.

Several recent developments in numerical flow simulation suggest the emergence of an alternate paradigm, here termed 'autonomous microstructure evolution' (AME). In Sect. 1.2, this paradigm is introduced by describing several methods of this type. The focus of this chapter is the proposal of a new AME-type method for simulation of turbulent flows that is based on a stochastic model, 'one-dimensional turbulence' (ODT).

After introducing the AME paradigm, its desirable attributes from the perspective of turbulence modeling are outlined in Sec. 2. The remainder of the chapter describes the proposed simulation method.

1.2 Autonomous Microstructure Evolution

At the molecular level, viscous fluid flow is strictly a local process. Molecular collisions are the elementary mechanism of momentum and heat transfer,

and they likewise control mass transfer, flow energetics, and chemical change in reacting flows. This is recognized in derivations of the continuum equations of fluid flow (e.g., the Navier–Stokes equation) from kinetic theory using elementary statistical hypotheses (e.g., the Boltzmann chaos assumption).

Accordingly, the continuum equations governing compressible fluid flow are local in nature. However, in low-Mach-number flows (Ma $\ll 1$), the sound speed becomes irrelevant to the dominant flow processes and it is physically more appropriate, and computationally more efficient, to adopt an incompressible formulation. This formulation treats the sound speed as effectively infinite and thereby allows flow evolution to be represented as an elliptic problem, in which all fluid elements and constraints (e.g., boundary conditions) are coupled instantaneously.

At this level of description, it is entirely appropriate, and generally quite advantageous, to dispense with the local character of the physical processes that govern low-Ma flow evolution. However, there is an alternative, local formulation that is sometimes advantageous at low Ma, called the pseudo-compressible formulation [1]. In this formulation, an artificially low sound speed is introduced in order to reduce the time-scale disparity between acoustic and solenoidal flow processes, thus mitigating the severe time-step constraints for compressible-flow time advancement at low Ma.

To summarize, the continuum-level governing equations need not obey locality in order to capture the governing physics at low Ma, although a local formulation may be a viable option. These considerations provide a useful context for defining and illustrating the AME paradigm.

The most direct way to simulate fluid flow is to remain as faithful as possible to its occurrence in nature, i.e., by simulating the underlying molecular motions and interactions. The most common and successful method of this type is 'molecular dynamics' (MD) [2, 3], whose virtue in this regard is that it captures non-continuum effects when they are important, as well as flow evolution describable by continuum methods.

MD in this context is a direct molecular simulation, subject to idealization of molecular collision processes, e.g., through the adoption of a molecular pair potential. However, the MD concept has been generalized through the development of models in which computational molecules are pseudo-particles. Their properties and interactions are defined so that macroscopic flows can be simulated using much fewer than Avogadro's number of particles. Examples of this approach are 'smoothed particle hydrodynamics' (SPH) [3] and 'dissipative particle dynamics' (DPD) [4]. Another method of this type is 'lattice-gas hydrodynamics' (LGH) [5], whose distinguishing feature is that it is designed to yield controlled (i.e., arbitrarily accurate) approximations to the continuum governing equations although the particles do not represent physical molecules.

The common feature of the methods described thus far, and the method proposed here, is that a representation, exact or idealized, of small scale processes is adopted that yields, through process evolution, collective behaviors

that correspond to continuum flow, with varying degrees of accuracy. This is the defining feature of the AME paradigm in the context of flow simulation.

Another AME-type method, the 'lattice Boltzmann model' (LBM) [5], illustrates that these methods are not exclusively particle-based. LBM evolves probability density functions (PDFs) of particle properties rather than particles *per se*. It thus retains a link to particle properties though particles are not explicit within the method. In this regard it may be viewed as intermediate between particle and continuum methods. Another notable feature of LBM is that turbulence modeling has been incorporated into the LBM framework [5].

The link between LBM evolution and the implied particle evolution can be formalized by noting that evolution of a PDF represents the ensemble evolution of a collection of particles governed by coupled stochastic differential equations (SDEs) . In this context, the latter is a more detailed level of description from which the former can be deduced. However, in a class of turbulent flow models, the relationship is reversed. An unclosed hierarchy of evolution equations for the PDF of flow properties in turbulence can be closed by modeling to obtain a single-point evolution equation for the joint PDF of velocity and scalar fields [6]. Though elliptic in character in its usual low-Ma formulation, it can be solved using a algorithm of AME type. Namely, particle SDEs are formulated whose details, apart from the conformance of their ensemble properties to the PDF evolution equation, need not be physically realistic. These SDEs are solely numerical devices for efficient solution of the PDF evolution equation. In this sense, they are analogous to LGH, in which particle evolution is strictly a device for solving continuum equations, albeit the exact equations in that case.

The foregoing AME-type methods, whether used as complete (particle through continuum regime) flow simulations (e.g., MD), as numerical devices for solving exact or modeled continuum equations, or as models in their own right, are all explicitly or implicitly particle based. The AME paradigm also accommodates processes rather than particles as its primitive elements. A notable example is vortex dynamics (VD) [7], which in its two-dimensional (2D) implementation evolves discrete point vortices or vortex blobs. (In 3D, the vortex filaments, arrows, and particles have been used [7]–[9].) The Biot–Savart equation that couples the discrete elements is non-local, illustrating that the AME paradigm is not limited to local interactions. Vortex dynamics is generally applied to low-Ma flow, and captures the non-locality of that flow regime in a natural way. In 2D flow, the large-scale organization of vorticity is elegantly reproduced by discrete-vortex simulations. To represent unresolved motions in VD simulations of turbulence, vortex blobs can execute random walks and/or undergo evolution of their internal structure (vorticity profile).

The formulation proposed here is akin to VD in that its primitive elements are processes rather than particles, and as in VD, a process represented in this manner introduces some form of non-locality. As in VD, the primitive elements are associated with vortical motion, but unlike the discrete vortices of VD, they represent the outcome of vortical motion rather than vortices

per se. Closely related to this distinction is the key attribute of the primitive elements introduced here: they are processes implemented on a 1D spatial domain.

2 Implications for Turbulent Flow Modeling

2.1 Large-Eddy Simulation: Capabilities and Limitations

The motivation for adopting the AME paradigm for turbulent flow modeling, and implications concerning the structure of such a model, are now considered. These questions are addressed by first examining the conventional paradigm outlined in Sect. 1.1.

Specifically, consider 'large-eddy simulation' (LES) of constant-property flow. The LES strategy is to resolve scales far enough below the flow-dependent energy-containing scales so that the unresolved motions are within the inertial sub-range, whose properties are presumed to be universal [10]. Moreover, the main role of the unresolved motions is presumed to be cascading of mesh-resolved kinetic energy to smaller, unresolved scales. This is represented within LES by dissipation of mesh-resolved kinetic energy, at a rate commensurate with the cascading mechanism. The dissipation is typically incorporated using eddy viscosity, or a generalization thereof (tensor viscosity, spectral viscosity, etc.) [10].

Though this strategy has proven to be quite successful thus far and holds great promise for the future, it is subject to two types of limitations that motivate consideration of an alternative approach. One type of limitation is generic to all applications of this strategy, while the other type is flow specific.

The generic limitations are associated with the LES representation of cascade physics. Intermittency of the turbulent cascade [11] has several consequences whose representation within LES is not yet fully satisfactory. One is backscatter of kinetic energy from unresolved to resolved scales. Modeling of backscatter within LES is an active research topic, and there has been useful progress in this regard [10]. Another is a spectrally non-local contribution to downscale (forward cascade) energy transfer. Spectral viscosity methods can account for this, but are not necessarily advantageous or practical from other viewpoints. Intermittency effects depend on the turbulence Reynolds number Re in a manner that has not yet been convincingly captured as LES is applied to flows at successively higher Re [12].

Apart from these physics concerns, there is the practical concern of devising an LES closure that is numerically robust within the time advancement of a non-smooth discretized velocity field as well as physically sound. There is room for improvement in this regard as well.

These limitations arise in the context of applications that satisfy the basic axiom of the LES strategy: mesh refinement sufficient to resolve flow-specific

phenomena. There are (at least) two classes of applications that challenge this axiom: wall-bounded flows and flows coupled to dissipation-scale processes.

In wall-bounded flows, the scale of near-wall flow-specific phenomena is proportional to distance from the wall, hence decreases as the wall is approached, until the viscous sub-layer is reached. This requires refinement to full flow resolution, in effect, direct numerical simulation (DNS), near walls in order to maintain fidelity consistent with the LES strategy. Though costly, this near-wall refinement may be feasible for some applications. In general, however, the cost of this approach is prohibitive, so instead, near-wall parameterizations are introduced. The consequences of introducing parameterizations are considered shortly, after other examples of parameterization are noted.

Those examples are parameterizations that represent the coupling of unresolved flow scales to dissipation-scale (or in general, subgrid-scale) processes, such as thermodynamic fluctuations (in compressible flow), mixing of dynamically active scalars (e.g., density in buoyant variable-density flow), chemical reactions (including heat-release effects on density and hence on the flow field), and multiphase couplings. Multiphase couplings include diverse phenomena such as momentum, heat, and mass transfer between dispersed and continuum phases, and surface tension at interfaces between immiscible liquids.

The limitations of parameterizations of these coupled, highly nonlinear, multivariate, spatially distributed processes are well known and are not elaborated here. Certainly, they are at least as challenging as the parameterization of near-wall constant-property flow, so the latter is examined to illustrate the difficulties that can arise.

In near-wall flow, an obvious modeling concern is prediction of separation and reattachment. One mitigating factor in an LES formulation is that adaptive meshing can resolve the vicinities of separation and reattachment loci along a wall at much less cost than than resolving the entire near-wall flow. An application that is less amenable to adaptive meshing is near-wall flow subject to transient bulk forcing. An example is near-surface flow in the atmospheric boundary layer (ABL) subject to shifts of wind speed and direction. The time-lagged response of the near-wall flow to this transient forcing can, for example, result in non-monotonic wall-normal profiles of ensemble-averaged velocity components, and related flow-specific features, that defy representation by a parameterization. (Another canonical example of near-wall non-monotonicity is buoyancy-driven flow near a heated vertical wall.)

This considerations point inexorably to the conclusion that parameterization of unresolved flow-specific phenomena, in contradiction of the axiom underlying the LES modeling strategy, imposes inherent limitations on the breadth and accuracy of predictive capability that this strategy can ultimately achieve. Within the scope of these limitations, much can and will be accomplished. Nevertheless, it is apparent that there is a compelling fundamental as well as practical imperative to pursue alternate strategies that might not be subject to these limitations.

2.2 An Alternative to Parameterization

It is useful to define what is meant by parameterization in order to delineate a possible alternative. Here, a broad definition is adopted. Namely, a parameterization is any mathematical construct associated with a mesh control volume (or more generally, a localized stencil of control volumes) that exchanges information during the simulation only with values of mesh-resolved variables in that control volume (or stencil). This definition includes some formulations that are termed 'dynamically active' LES subgrid models [10]. Here, the distinguishing feature is taken to be the nature of the communication among modules (i.e., the flow solver and the parameterization) rather than the internal content of the parameterization.

This definition is adopted because it addresses the strategy of devising better parameterizations. One can in principle improve the parameterization to the point of performing DNS within each control volume. Nevertheless, this is not equivalent to DNS of the whole flow if the information exchange between control volumes is based solely on mesh-resolved variables. This restricted information exchange introduces an inherent information loss that does not occur in whole-flow DNS.

In this regard, it is useful to compare constant-property LES of unbounded flow to the more challenging cases discussed in Sect. 2.1. The downscale information transfer in LES is straightforward in principle because it involves the loss of information (about flow structure whose scale is compressed below the resolution scale) that is no longer needed in the simulation (if only the forward cascade is considered). The upscale information transfer is a more delicate issue because it requires retention of subgrid-scale information (e.g, by using a parameterization) that is sufficient to characterize backscatter through transfer of this information to the resolved variables. On this basis, upscale transfer is generally viewed as a more challenging modeling problem than downscale transfer.

Compare this to the modeling requirements for more complicated flows (variable property, chemically reacting, etc.), supposing in these cases that an elaborate, accurate parameterization is available. For quantities such as chemical species in a reacting flow, the upscale information transfer may consist of a straightforward averaging or spatial filtering procedure. However, the downscale information transfer may require, for example, adjustment of small-scale species concentrations resolved by the parameterization, where the adjustment is based on spatially filtered information at the mesh scale. This adjustment can be problematic with regard to either realizability (e.g., causing mass fractions to be negative or exceed unity) or chemical consistency (e.g., creating spurious non-equilibrium mixtures).

Thus, as subgrid parameterizations become more elaborate in order to address increasingly complex problems, the fidelity of the overall formulation may be constrained, to an increasing degree, by the sparse information content (relative to the subgrid formulation) at mesh-resolved scales. It can be

anticipated that this problematic downscale information transfer will prove to be the most enduring constraint on the ultimate utility of parameterization, as broadly defined here.

Accordingly, the basic axiom that guides the present pursuit of a better alternative is that parameterization requiring downscale information transfer should play a minimal role, if any. AME, as defined and exemplified in Sect. 1.2, is precisely the paradigm that adheres to this principle.

Adopting the AME paradigm on this basis, a formulation of this type is desired that preserves the essential characteristics of AME as it is generalized to multi-physics problems. As noted in Sect. 1.2, LBM and VD have been applied to turbulence by appending treatments that are parameterizations (as defined here) underneath the model. These extended formulations are thus hybrids that are subject to the same limitations as other parameterizations.

This is a generic outcome of efforts to isolate the model representation of individual sub-processes within limited scale ranges. As this inference suggests, a robust remedy would be to implement all sub-processes at all scales. Superficially this defines DNS, which is fully accurate but unaffordable for most problems. However, there is an alternate, more affordable realization of this strategy. Namely, implement all sub-processes at all scales in a lower-dimensional space. 2D examples of dimension reduction include VD and 2D Eulerian solution of the exact evolution equations. However, 2D turbulence has qualitatively different characteristics from 3D turbulence, in addition to the obvious limitation that general 3D initial and boundary conditions cannot be represented in 2D.

Nevertheless, there is a form of dimensional reduction that can both preserve the physics of 3D turbulence and accommodate general 3D flow configurations, while providing an all-scale representation of all sub-processes. Description and assessment of this formulation is the focus of the remainder of this chapter.

2.3 Superparameterization and Its AME Reformulation

Simulation of global atmospheric circulation is a salient application that confronts the challenges outlined in Sects.2.1 and 2.2. An emerging strategy for addressing this problem exemplifies the all-scale AME paradigm. An important caveat in this context is that geophysical-scale flows cannot be affordably simulated with resolution to viscous scales, even in a formulation with reduced dimensionality. However, the modeling concept can be recast so as to obtain a fully resolved formulation applicable to engineering-scale flows.

The AME-type atmospheric simulation strategy is a variant of 'superparameterization' (SP) [13]. As noted in Sect. 2.2, the ultimate parameterization is a DNS associated with each mesh control volume. A step back from this would be a fully resolved 2D simulation associated with each mesh control volume. The qualitative as well as quantitative limitations of 2D simulations (Sect. 2.2) would counteract the benefits of this degree of detail for many

applications. However, for typical convective flow regimes in the ABL, 'cloud-system resolving models' (CSRMs) implemented on planar vertically oriented domains have proven to be cost-effective alternatives to 3D simulation [14]–[16]. In effect, 2D is found to be the dimensionality that optimizes the cost-performance tradeoff for this class of flows. Accordingly, SP implements a 2D CSRM-type simulation associated with each control volume of a general circulation model (GCM) of the Earth's atmosphere.

SP as such is subject to the inherent limitations of parameterization, but a variant of this formulation that adheres to the AME paradigm is under development [17]. To visualize this variant, imagine that the CSRM simulations tile the vertical faces of the GCM control volumes in a hypothetical Cartesian geometry involving one planar layer of rectangular GCM control volumes. Thus, the control volume height is the vertical extent of the simulations. Instead of implementing an independent CSRM on each vertical control-volume face, suppose that a CSRM is implemented on each 2D domain corresponding to a vertical sidewall of each row or column (the two horizontal coordinates) of the array of GCM control volumes. Then the height of each CSRM domain is the vertical extent of the simulated atmosphere, and its horizontal extent spans one of the two horizontal directions (e.g., the Earth's circumference if the given direction is the Cartesian analog of a great circle). With a suitable coupling among these 2D domains, it is possible (and desirable, for the reasons explained in Sect. 2.2), to dispense with the GCM itself and thus obtain an AME-type formulation, which is denoted here as 'super-AME' (SAME).

2.4 A 1D AME Formulation

Having presented the rationale for the AME paradigm and the main elements of its implementation for a particular application, adaptations for other purposes are considered. As in the atmospheric flow application, a key consideration is the spatial dimensionality that is most cost-effective for a given application.

There are several applications for which a 1D formulation is advantageous in principle. One is wall-bounded flow, in which evolution of the wall-normal profile of flow properties embodies the dominant physics. Analogously, thin free shear flows (e.g., jets, wakes, and mixing layers) are boundary-layer type flows whose representation based on property profiles along a lateral coordinate is common [18]. Another such application is horizontally homogeneous vertically stratified buoyant flow. 'Single-column models' (SCMs) are vertically oriented 1D formulations that are commonly applied to ABL flows of this type [16]. Finally, 'stationary laminar flamelet models' (SLFM) used in turbulent combustion simulations involve 1D (flame-normal) flow representations [19].

The 1D formulation described here has been applied to all these flow types. Representative results are discussed in Sect.7. For now, the utility of a 1D for-

mulation is assumed, deferring the question of how turbulence can be modeled in 1D until Sect. 5.

Given such a 1D model, there are several ways that it can be used in the construction of a 3D simulation. One way is to associate a 1D line segment, on which the model is implemented, with each control volume of an LES, analogous to one of the ways of incorporating CSRMs into a GCM (Sect. 2.3). This 1D analog of SP might be termed 'semi-superparameterization' (SSP) because the subgrid model dimensionality is half that of SP. Extending the analogy, assume a Cartesian mesh of cubic LES control volumes. Consider the rectangular volume formed by a linear stack of LES control volumes in any one of the three coordinate directions (analogous to a row or column of GCM control volumes). Now take each side-edge of each of these rectangular volumes to be a 1D domain for implementation of the 1D model of turbulence. Each of these domains then spans the flow in a given direction, and is presumed to resolve all relevant length scales. Thus it has the needed attributes for an all-scale AME-type formulation, subject to the specification of suitable rules for coupling the various domains. This is the 1D analog of SAME (Sect. 2.3). For consistency with terminology used previously [20], this 1D methodology is denoted ODTLES, while SSP and related 1D formulations are denoted LESODT. Despite the terminology, ODTLES is an AME formulation that does not involve the advancement of LES-type equations, just as SAME (Sect. 2.3) dispenses with the GCM machinery.

2.5 Hybrid Formulations

Section 2.2 alludes to two of the many possible hybrid formulations that combine attributes of the approaches mentioned thus far. Description of all the promising possibilities is beyond the scope of this chapter, but a particular hybrid formulation that is based on the modeling approach discussed in Sect. 4.2 is mentioned here.

The distinction between parameterization, in which information is transferred between different scale ranges, and AME, in which all information transfer involves spatially resolved quantities, has been emphasized thus far. For some applications, it is advantageous to evolve some variables using parameterization and evolve others with full resolution. A variant of the domain geometry described in Sect. 2.4 with reference to SSP (nominally a parameterization) has in fact been implemented as a hybrid of this type [21, 22]. Namely, for combustion simulation, thermochemical information (species mass fractions and enthalpy) resides solely on the 1D line segments, while momentum and pressure reside on the coarse 3D mesh. The upscale information transfer consists of density changes that drive the mesh-resolved advancement of the continuity equation. The downscale transfer consists of velocities normal to control-volume faces. These velocities prescribe volume transfers, in a Lagrangian sense, between 1D segments associated with control volumes

that share a common face. This Lagrangian transfer operation, termed 'splicing,' preserves chemical states, thereby mitigating the inherent artifact of reacting-flow parameterization (Sect. 2.2). It also preserves small scale spatial structure, subject to an important caveat. In a receiver segment, newly spliced fluid from a donor segment contacts receiver fluid at one location, possibly creating an unphysical local configuration (e.g., cold fuel in contact with cold air under physical conditions that would require flame at all fuel-air interfaces). This is the first of several illustrations that dimensional reduction involves compromises and trade-offs, as in any modeling approach. Nevertheless, splicing is an advective transfer rather than a surrogate mixing operation, so it preserves local chemical states. The only species mixing in this formulation is by a physically accurate molecular mixing process, in contrast to models that are strictly parameterizations.

Among the various proposed model formulations encompassed by the rubric 'superparameterization' are some that would be termed hybrids in the present classification [17]. It can be anticipated that the distinct but overlapping interests of the geophysical and engineering fluid dynamics communities (as well as the astrophysics community, whose interests are discussed elsewhere in this volume) will stimulate a productive cross-fertilization of modeling concepts as progress continues in these arenas.

3 Proposed Modeling Strategy

3.1 Overview

The goal of this chapter is to outline a turbulence simulation strategy in which ODT is a central element, and in so doing, to motivate as well as explain ODT. The strategy as outlined has not yet been implemented computationally, although an effort to do so is underway and development of several key components of the strategy has been completed.

Section 1 introduces the AME paradigm and explains its advantages for turbulent flow simulation. The strategy outlined here is designed with this in mind, subject to the inevitable compromises involved in modeling.

In Sect. 2.4, the 1D domain is defined geometrically as a line segment, specifically, a line segment corresponding to an edge of a linear stack of cubic control volumes (CVs). This is useful conceptually, but for numerical implementation, it is preferable to interpret 1D model evolution as occupying a volume of space, enabling a finite-volume numerical representation. For this purpose, the rectangular volume occupied by each stack of control volumes within the 3D domain is taken to be a 1D model domain.

In particular, assume that the 3D flow domain is itself rectangular, with coordinate bounds $0 \le x \le X$, $0 \le y \le Y$, and $0 \le z \le Z$. This geometry corresponds to a proof-of-principle application proposed in Sect. 7.1, but for

now it is illustrative. Assume nominal CVs (whose role, in the absence of mesh-scale advancement, is as yet unexplained) that are cubic with edge length M. X, Y, and Z are all assumed to be integer multiples of M, so the flow domain can be tiled with a cubic array of these CVs. For convenience, express length in units of M, so X, Y, and Z are integers. Then the CVs in the array are indexed (i, j, k), where $1 \leq i \leq X$, $1 \leq j \leq Y$, and $1 \leq k \leq Z$, and the respective CVs are denoted C_{ijk}.

CVs stacks, each of which is a 1D model domain as defined above, are formally defined as $\bigcup_n C_{ijk}$, where n denotes either i, j, or k. For example, $S_x(j,k) = \bigcup_i C_{ijk}$ is the index-(j,k) stack oriented in the x direction, which is then the coordinate direction of the 1D model implemented on $S_x(j,k)$. $S_y(i,k)$ and $S_z(i,j)$ are defined analogously, yielding three arrays of stacks oriented in the respective coordinate directions. Each array fills the flow domain. Likewise, each CV C_{ijk} is contained in three stacks.

In the proposed formulation, three distinct flow solutions are time-advanced concurrently, each in one of the stack arrays. Each is a self-contained solution in that it does not exchange fluid or fluid properties with the other solutions, but the solutions are coupled in that each determines fluxes that are used to close the other two solutions. Each solution is designated by the corresponding subscript of S, i.e., x, y, or z.

Now consider the sub-structure of each stack, or 1D domain. (These terms are used interchangeably.) An x-oriented stack, or x-domain, is considered for illustration. (In general, statements about x-domains are likewise applicable to y-domains and z-domains.) By definition, each x-domain has sub-structure consisting of linear array of X cubic CVs, each of edge unity in the chosen scaled units. The first and last CVs each have one face interior to the x-domain, four contained in its respective side-faces, and one coinciding with an end-face of the x-domain. The other CVs in the x-domain each have two faces interior to the x-domain and four contained in its respective side-faces. The union of non-interior CV faces coincides with the surface of the x-domain.

The CVs are central to the coupling of the three concurrent flow solutions. Additional x-domain sub-structure needed to advance the individual solutions is now introduced.

The x-domain is already partitioned into X CVs by the CV interior faces. A refinement of this partitioning is introduced. Parallel to those interior faces, additional faces are introduced so that the x-domain is partitioned into mX cells of identical shape, denoted 'wafers,' where m is an integer. The x-domain is now a linear array of mX wafers of edge $1/m$ (in scaled units), such that the union of each successive set of m wafers coincides with a CV. Each wafer is a rectangle of dimensions $(1/m) \times 1 \times 1$, where in general $m \gg 1$, hence the terminology.

This x-domain refinement defines a mesh, resolving the length scale $\Delta x = 1/m$, on which the 1D model is implemented. This is the length scale at which the flow is resolved within the 1D treatment. 3D flow is captured explicitly at length scales above unity through the coupling of flow solutions. Below

length scale unity, 3D flow is captured only to the extent that it is represented implicitly within the 1D model. (See Sect. 3.2.) If the CVs formed the mesh for an analogous explicitly 3D flow simulation, then the range of represented scales would be 1 through X. In the present formulation, an additional factor m of scale resolution is introduced through modeling. Because this additional resolution is introduced in 1D rather than 3D, the number of computational cells in the simulation is smaller, by a factor of order m^2, than the number required for equivalent 3D resolution. The attendant computational cost reduction is the benefit of the present formulation. The trade-off for this cost reduction is the use of a model, rather than the exact governing equations, to evolve the flow at scales smaller than unity.

Commensurate with the disparate scales at which the flow is resolved in 1D and in 3D, the time step for advancement of the 1D model on an x-domain is considerably shorter than the time step for coupling of the three flow solutions. Therefore, 1D model advancement is sub-cycled within an overall time-advancement cycle whose time increment corresponds to the solution-coupling time step. (If fractional-step advancement is used, there may be several coupling operations per time-advancement cycle. Numerical implementation is not considered here at this level of detail.) The advancement cycle is explained further in Sect. 3.3.

Several aspects of numerical implementation are noted. First, during 1D sub-cycling, each x-domain evolves autonomously. This provides an efficient domain decomposition for parallel implementation that should yield near-perfect scalability owing to the predominant cost of 1D sub-cycling relative other operations during the advancement cycle. Second, spatial uniformity of the 1D refinement of the x-domain has been introduced for clarity of exposition. Though this meshing is used in 1D model applications reported to date, an adaptive-mesh formulation presently under development offers the possibility of substantial cost savings that will extend the range of applicability of this formulation. (See Sect. 6.1.) Third, the advancement cycle as outlined excludes any advancement sub-processes on the 3D mesh (union of CVs). If an incompressible formulation of the momentum equation were adopted, then enforcement of continuity would require an elliptic solve of the pressure Poisson equation, contravening the AME paradigm. A formulation of this type has in fact been implemented [20], as discussed in Sect. 6.3. For the purpose of formulating a model within the AME paradigm and noting its attributes, a compressible analog of that incompressible formulation is proposed here.

3.2 1D Advancement

The 1D sub-cycling on each x-domain is both the novel feature and the main physical content of the proposed formulation, so it is explained in detail in Sect. 5. Here, the 1D modeling concept is introduced briefly.

Within the proposed compressible-flow treatment, a natural context for 1D modeling is 1D gas dynamics [23]. In general, 1D gas dynamics is a steady-

state formulation useful for analysis of shocks and other high-Ma phenomena. Here, compressibility is introduced in order to exploit its technical advantages for turbulent flow simulation, as in [24], rather than for investigation of high-Ma phenomena *per se*.

Starting from conventional 1D gas dynamics, possible extensions to represent turbulent flow effects are considered. Steady-state representation of compressible as well as incompressible turbulent flow is provided by 'Reynolds-averaged Navier–Stokes' (RANS) formulations. For compressible flow, the simplest of these formulations introduce an eddy viscosity and an eddy diffusivity (for temperature). Similarly, one can introduce eddy transport coefficients within (otherwise inviscid) 1D gas dynamics.

The utility of such a formulation as a self-contained model of compressible turbulence is questionable. However, the purpose of a 1D compressible turbulence formulation in the present context is not to obtain a self-contained model, but rather, to obtain a sub-model suitable for the proposed 3D AME framework.

Moreover, 1D gas dynamics with eddy transport does not in itself address the present need. Operationally, eddy transport is a diffusive process that smooths fluctuations rather than generating or sustaining them, contrary to the present goal of explicitly simulating small scale turbulent fluctuations.

In this regard, recall the discussion in Sect. 1.2 of the relationship between PDF evolution equations and SDEs. Turbulent transport, which is diffusive in an average sense (and is represented diffusively in PDF as well as in RANS turbulence models), can be represented a fine-grained sense by SDEs. However, as noted in Sect. 1.2, if the SDEs are formulated in conformance to model-based PDF evolution equations rather than the exact governing equations, the resulting fine-grained representation may not be physical, and in fact, generally isn't. (It is noted in passing that this caveat applies also to LGH. Although LGH solves equations that are exact at the continuum level, local particle fluctuations correspond in this instance to a postulated sub-continuum dynamics that is not intended to be an accurate representation of molecular fluctuation effects.)

In fact, there is a generic difficulty with the introduction of fine-grained structure using SDEs. SDEs are driven by noise fields that are difficult to constrain so that they obey global conservation laws, which require the constancy of spatial integrals over specified functions of the noise, the dependent variables, or both. For applications involving separation of length scales, such as the thermodynamic or hydrodynamic limit of statistical mechanics, this does not necessarily cause a problem. For example, if molecule numbers in a set of control volumes are allowed to fluctuate individually (e.g., Poisson shot noise reflecting local density fluctuations), the constancy of total molecule number in the whole system, which holds for a closed system with no chemical reactions, is not enforced. However, in the thermodynamic limit, the stochastic model describes a grand canonical ensemble that either converges to the be-

havior of the physically correct canonical ensemble or can be used to infer properties of the true physical system.

There is no separation of length scales in turbulent flow and hence no freedom to deviate from global constraints, but there are ways to incorporate conservation constraints in particular cases. For example, an SDE for the stream function can be used to introduce velocity fluctuations while preserving continuity in 2D. (The relationship between velocity and stream function in 2D assures that the flow remains solenoidal [25].) However, there is no obvious way to use SDEs to obtain a reasonable fine-grained 1D representation of turbulence that obeys applicable conservation laws. In this regard, the stochastically forced Burgers equation [26], though in many ways an illuminating 1D analog of turbulence, is manifestly incapable of evolving fluid density in conformance to a specified equation of state.

Thus, the utility of SDEs for modeling the small scales of turbulence is not precluded, but an SDE formulation suitable for present purposes has not been identified. On physical grounds, there is an inherently more robust approach.

The compressible flows of interest here involve both solenoidal and dilatational motions. The dilatational motions represented during 1D sub-cycling are governed by conventional 1D gas dynamics (Sect. 5.4). Dilatational motions not included within this representation are captured during solution coupling (Sect. 3.3). To be captured in a 1D formulation, solenoidal motions require special treatment, as follows.

Consider the advancement, for a time Δt, of the advective operator in the equation of motion for any property field $\theta(\boldsymbol{x},t)$, assuming numerical operator splitting so that other evolution processes (e.g., molecular transport) are omitted. This advancement is equivalent to a mapping $\boldsymbol{x} \rightarrow \boldsymbol{x}'(\boldsymbol{x})$ of each location $\boldsymbol{x}$ to a new location $\boldsymbol{x}'$. The corresponding transformation of θ is $\theta(\boldsymbol{x}) \rightarrow \theta(\boldsymbol{x}'(\boldsymbol{x}))$. This specifies the transformed θ field as a function of the coordinate $\boldsymbol{x}'$ at the new time by setting θ at new location $\boldsymbol{x}'$ equal to the θ value at the old time at the location $\boldsymbol{x}$ that is mapped to $\boldsymbol{x}'$ by the advancement operation.

This rather elaborate representation of advection, whose conventional representation is the $\boldsymbol{v}\cdot\nabla$ operator, is introduced because the two are not equivalent, but rather, the former is a *generalization* of the latter. To see that the former includes the latter, integrate the Lagrangian advective equation $d\boldsymbol{x}/dt = \boldsymbol{v}(\boldsymbol{x},t)$ from t to $t+\Delta t$ to obtain the mapping $\boldsymbol{x} \rightarrow \boldsymbol{x}'(\boldsymbol{x})$ that is equivalent to $\boldsymbol{v}\cdot\nabla$ advancement for a given $\boldsymbol{v}(\boldsymbol{x},t)$ space-time history.

The advantage of the map representation of advection is that it can be used to formulate models that decompose the advection process into a sequence of discrete operations that advance property fields over any specified time interval, e.g, finite rather than infinitesimal. This decomposition can replicate physical advection exactly if the map is based on integration of the exact Lagrangian advective equation for given $\boldsymbol{v}(\boldsymbol{x},t)$ over a finite time interval Δt. However, if $\boldsymbol{v}(\boldsymbol{x},t)$ is not known *a priori* because fully resolved advancement of the exact 3D governing equations is unaffordable, then a map represen-

tation based on a postulated stochastic process can be used to model this advancement.

Stochastic iterated maps are in fact familiar tools of statistical mechanics modeling, including turbulence models [27, 28]. The noteworthy feature here is the application of the maps to the independent variable $\boldsymbol{x}$ rather than to the dependent variable θ. This approach allows incorporation of features of advection that are needed for physically sound flow simulation.

In VD (Sect. 1.2), the continuum process of vortical advection is spatially discretized but advanced in continuous time. The map representation of advection likewise enables discretization of a continuum process, in this case in the time domain. The specific map *ansatz* that is introduced is analogous to the individual vortex blob in VD in that it is applied to a finite spatial region and is intended to represent an elementary fluid motion ('eddy') in turbulence. However, a vortex blob can persist indefinitely (although some VD implementations allow blob merger) and execute any number of circulations, but each map is a one-shot event representing a particlar displacement field ($\boldsymbol{x}' - \boldsymbol{x}$ as a function of $\boldsymbol{x}$), e.g., one circulatory motion.

Map-based advection modeling, applied in 3D, yields novel mathematical insights as well as an efficient simulation method for a class of turbulent multiphase processes [29]. For present purposes, the key point is that map-based advection can be applied in 1D.

In 1D, the only solenoidal flow that can be generated by the $\boldsymbol{v} \cdot \nabla$ operator is rigid translation. In map language, the solenoidal property can be stated as follows: $\int_{\sigma'} dx' = \int_{\sigma} dx$ for any subset σ of x, where σ' is the image of the subset σ obtained by the transformation $x \to x'$. (Henceforth, boldface is omitted in statements specialized to 1D, although in this and some other cases the validity of the statement is not restricted to 1D.) This is a statement of measure preservation by the map. It is more general than the usual solenoidal condition $\nabla \cdot \boldsymbol{v} = 0$ because it encompasses a more general class of advection processes. The existence, within the map representation of advection, of non-trivial 1D motions that are measure preserving, and obey another essential property, is the key motivation for introducing map-based advection here (although it is likewise useful in 3D, as noted).

The other essential property is a particular form of continuity. It is different from adherence to the continuity equation, which reduces, for incompressible flow, to the solenoidal condition. Here, continuity refers to the relation

$$|x(x'_1) - x(x'_2)| \leq B|x'_1 - x'_2|, \tag{1}$$

where subscripts denote particular values of x', and B is a finite numerical constant; for the map *ansatz* adopted here (Sect. 4.2), $B = 3$. Equation (1) ensures that the map does not introduce spatial discontinuities into a continuous function, i.e., $h(x') \equiv g(x(x'))$ is continuous in x' if $g(x)$ is continuous in x.

It is important to enforce this form of continuity, not only because it is obeyed by the exact equations of motion (except for inviscid compressible

flow, which is not considered here), but also because violations of this condition can introduce significant artifacts. Velocity discontinuities correspond to infinite local strain and thus, unphysically large local turbulence production. A possible anomaly resulting from species concentration discontinuities is noted in Sect. 2.5.

These artifacts can be remedied to some extent, but there is a more fundamental reason for enforcing (1). The coefficient B in (1) bounds the multiplicative decrease in separation that a map can induce between a pair of fluid elements (here meaning fluid states at particular points in space). Central to turbulent cascade phenomenology is the notion of locality of the turbulent cascade in scale space, i.e., individual fluid motions in turbulence (eddies) induce at most order-unity reduction of fluid-element separation [11]. Intermittency suggests deviations from this picture that can be interpreted within the present framework as locally large values of B. The mapping *ansatz* has been formulated in way that accommodates this [30], but implementations to date conform to (1) with $B = 3$, and in one instance $B = 5$ [31].

Formally, a map represents a change of configuration corresponding to some time increment Δt. It would therefore appear that a time update should be associated with map implementation. However the formulation does not accommodate this for several reasons. First, maps are applied to finite spatial regions, representing the spatial extents of individual turbulent eddies within the 1D representation. In turbulence, many eddy motions are occurring at a given instant, implying multiple overlapping time increments, if a corresponding literal time advancement is triggered by each map. This leads to conceptual as well as computational difficulties. Second, the intent is to model all physical processes subsumed in the governing equations, not solely advection. There is no plausible way to time advance, e.g., diffusive transport, as a sub-cycling process within a map representation of an eddy because a map is inherently instantaneous. Hence, the finite time duration of an eddy motion cannot be represented operationally within the model.

The physics associated with eddy time scales is nevertheless contained in the model, albeit in an indirect way that does not fully capture turbulence phenomenology. Operationally, 1D advancement consists of conventional advancement of sub-processes other than solenoidal advection, punctuated by instantaneous maps (with no associated time incrementation) representing the latter. This is equivalent to a sequence of initial-value problems, where the system state after a map is the initial state, which is advanced until the occurrence of the next map, which modifies the spatial structure of the dependent variables in some sub-region, thereby establishing initial conditions for further time advancement. The statistics of the time intervals between maps in various size ranges are the model representation of the temporal character of eddy motions.

Thus, within the 1D advancement there is an operator splitting, reflecting the qualitatively different model representations of solenoidal advection, consisting of maps, and other sub-processes. Between each map and the next,

the other sub-processes are sub-cycled; this might involve additional operator splitting based on numerical considerations. These other sub-processes correspond to 1D gas dynamics in the conventional sense, including dilatational flow aligned with the 1D domain (Sect. 5.4).

3.3 Advancement Cycle

A minimal description of the advancement cycle, omitting consideration of chemistry, output gathering, and related issues, is presented. As noted in Sect. 3.1, three distinct coupled flow solutions are advanced concurrently. For a given dependent variable θ, e.g., density or a velocity component, its state at a given time t is specified, for a given solution (e.g., the solution labeled x), as $\{\theta_{jk}(x,t)\}$, where $0 \le x \le X$, $1 \le j \le Y$, and $1 \le k \le Z$. Here, x is any real number in the specified range of the continuum 1D domain. For the discrete finite-volume formulation based on wafers of width $1/m$ (in the units of Sect. 3.1), in which x corresponds to wafer centers, x takes the values $(2n-1)/(2m)$, where n is an integer in the range $1 \le n \le mX$. The integer indices j and k label the θ profiles in the corresponding domains $S_x(j,k)$.

For the various dependent variables θ, this prescription fully specifies the states of the three flow solutions at time t. Note that no variables associated with the coarse CVs C_{ijk} are needed to specify the solution states. This is the hallmark of an AME-type formulation.

Initial and boundary conditions are specified with reference to individual property profiles $\theta_{jk}(x,t)$. For illustration, Rayleigh convection, a suitable target case for initial model application (Sect. 7.1), is considered. This flow is generated by holding each boundary of the rectangular flow domain at fixed temperature so at to induce gravitational instability, e.g., taking the bottom boundary ($z = 0$, where z is the vertical coordinate) to be at a given temperature T_0, while the other boundaries are held at some common temperature $T_1 < T_0$. No-slip conditions are applied at all these boundaries.

The simulation is run until a statistically steady state is reached, as measured, e.g., by velocity or temperature fluctuations at the center of the enclosure. Flow statistics are then gathered during statistically steady advancement. Therefore initial conditions are irrelevant. A simple choice of initial conditions is uniform temperature T_1 and motionless fluid throughout the domain.

Application of the boundary conditions is closely tied to the advancement cycle, which is now considered. Conceptually, though not necessarily in an efficient numerical implementation, the advancement cycle consists of two steps:

1. Sub-cycling, independently within all the domains $S_x(j,k)$, $S_y(i,k)$, and $S_z(i,j)$ of all three flow solutions, to advance the processes described in Sect. 3.2 from time t to time $t' = t + \Delta t$, where Δt is the advancement time step.

2. Property transfers across the boundaries of all the domains $S_x(j,k)$, $S_y(i,k)$, and $S_z(i,j)$ to enforce the equality of property fluxes across each CV face in the three flow solutions during the time interval Δt.

The significance of step 2 is illustrated by considering common face of CVs C_{ijk} and $C_{(i+1)jk}$. It is interior to $S_x(j,k)$ and on a lateral boundary of each of the domains $S_y(i,k)$, $S_y(i+1,k)$, $S_z(i,j)$, and $S_z(i+1,j)$. All three flow solutions require physically accurate property fluxes across this face during Δt. Step 1 induces property fluxes across surfaces interior to each 1D domain, but none across the lateral bounding surfaces of these domains, so these fluxes must be prescribed and implemented in some other way.

As the example illustrates, each CV face on a lateral boundary of a 1D domain is in the interior of a 1D domain of a different flow solution. Therefore properties are fluxed across that face during the step-1 advancement of the flow solution in which it is an interior face. These fluxes can be monitored during step-1 advancement of that flow solution.

The modeling assumption that closes the 3D formulation is that each property flux across a given CV face is the same in all three solutions. This implies, by Gauss' theorem, that all three solutions are the same at the mesh-filtered level unless property sources and sinks associated with 1D sub-cycling (step 1) are different within a CV for different solutions. This is possible in the present formulation, e.g., due to differing details of small scale mixing that affect chemical reaction rates locally. Mesh-filtered conserved properties evolve identically in the three solutions. (Here, filtering is a data-reduction technique rather than a part of the advancement algorithm.)

Thus, each property flux across a given CV face that is determined by one of the solutions during step 1 becomes a prescribed flux that, during step 2, governs transfer of the property across that face in the other two solutions. The step-2 transfers are between pairs of wafers in adjacent 1D domains, e.g., the 1D domain pair $S_y(i,k)$ and $S_y(i+1,k)$ in the example, and likewise, the 1D domain pair $S_z(i,j)$ and $S_z(i+1,j)$.

To specify the transfers in detail, consider the step-2 transfers of property θ across the common face of CVs C_{ijk} and $C_{(i+1)jk}$ in solution y. Let F be the θ flux across this face that is prescribed by solution x during step 1. Then for each integer n in the range $[1,m]$, the wafer values $\theta_{ik}(x,t)$ and $\theta_{(i+i)k}(x,t)$, where $x = i + (2n-1)/(2m)$, are incremented by $\pm f(x)\Delta t$, where $-$ and $+$ apply to the respective θ values and $f(x)$ is an interpolated flux constrained to obey $\sum_{n=1}^{m} f(x) = mF$. (Interpolants constrained in this manner have previously been used analogously [20, 32].)

The implementation of boundary conditions is essentially the same as the treatment of property fluxes at CV faces in the interior of the flow domain. Consider a CV face that is part of the flow boundary. The boundary condition at that face is applied during step-1 sub-cycling of the 1D domain that is bounded by that face and oriented normal to it. The flux of a given property θ through that face during step 1 is monitored, or it may have a known value

specified by the boundary condition. During step 2, this flux value F is an imposed flux across that face for the other two 1D domains that are bounded by the face. The interpolant f is constructed and θ values are modified accordingly, analogous to flux implementation across faces interior to the flow domain.

3.4 Relationship to Conventional Methods

The advancement cycle outlined in Sect. 3.3 is applicable irrespective of the details of the 1D advancement (Sect. 3.2). The fluxes during step 1 reflect contributions by molecular and advective transport, where the solenoidal part of the advective contribution is due to fluid displacements by maps. Alternatively, the solenoidal part could be based on a postulated eddy diffusivity. This representation of solenoidal flow on the 1D domain would smooth rather than wrinkle property profiles, so 1D mesh refinement ($m \gg 1$) would become spurious. Nevertheless, this alternative indicates the formal analogy, as well as the key physical distinction, between the present framework and conventional LES of compressible flow. The distinction is the resolution and explicit evolution, rather than smoothing, of small scale processes in the present formulation.

Not only is the present formulation formally analogous to LES; it can be rendered equivalent to an LES through constraints on the implementation of maps. As explained in Sect. 5, the map sampling process generates a distribution of map sizes that generally conform to the eddy size distribution inferred from conventional turbulence phenomenology. For a given magnitude of property gradient, the map-induced flux depends primarily on the size-vs.-frequency distribution of maps.

To render the model formally equivalent to LES, one can deviate from this physically based precription as follows. Characterize the overall magnitude of map-induced transport by an eddy diffusivity κ_e, which scales as ϕL^2, where ϕ and L are a representative frequency and size of the large eddies (i.e., the largest eddies implemented in 1D; see Sect. 6.2), which dominate transport. Assume that ϕ is increased and L is reduced so as to maintain constant κ_e, yielding many small eddies inducing the same transport as a smaller number of larger eddies. In the limit of diverging eddy frequency and vanishing L, the law of large numbers implies that fluctuations of property fluxes time averaged over the advancement step Δt vanish, so the stochastic model becomes deterministic. In this limit, the map sequence no longer induces physically relevant fine structure and its role is reduced to transport characterized by the diffusivity κ_e. Formally then, the model reduces to LES with an eddy-diffusivity closure, where the specific form of the closure depends, as in conventional LES, on how the dependence of κ_e on the flow state is specified. In this regard, the ODT eddy-selection process (Sect. 5.1) is closely analogous to conventional LES closure; see [33] for details.

Apart from its reduction to the physical modeling content of conventional LES, the present formulation requires an alternating-direction solution algorithm that differs from conventional LES numerics. Revision of the idealized advancement scheme of Sect. 3.3 can be anticipated as the algorithm is developed and tested.

This reduction to LES highlights the physical contribution of the map process when it has a realistic size-vs.-frequency distribution. As the scale L is dialed up from zero, fluctuations and associated fine-scale structure are introduced, but these properties do not necessarily enhance the realism of the model if the map distribution is not physically accurate. To benefit from this departure from an LES formulation, the induced fluctuations must be sufficiently accurate to provide a gain in model fidelity that justifies the computational cost of the method. This is best judged from the performance of the model. The particular formulation outlined here has not yet been implemented, but it is closely analogous to existing formulations. These are now considered in further detail in order to highlight the modeling concept and to assess how it might perform within the formulation proposed here.

4 Map-Based Advection Models

4.1 1D models of turbulent premixed combustion

Efforts by the author and co-workers to develop map-based methods for turbulent flow simulation in one or more spatial dimensions are summarized. The intent is to indicate the variety of possible formulations and the physics that is captured and omitted in particular instances.

The starting point was an effort to develop a minimal model of turbulent premixed combustion. The initial outcome was a formulation in which the instantaneous state of a turbulent flame is idealized as a bit vector (row of integers 0 or 1) in which each pair of adjacent bits interacts in two ways.

First, each 0 is converted into a 1 at a mean rate B times the number (0, 1, or 2) of adjacent bits in state 1. This process represents laminar burning with laminar flame speed BL, where L is the nominal spatial separation of adjacent bits. Note that there is some subtlety even at this level of description. The middle bit in a 101 configuration is deemed to burn twice as fast as in a 100 or 001 configuration because flames consume it from both sides, which is a reasonable but not uniquely plausible idealization of flame propagation. Also, this is a random process but could be plausibly formulated as a deterministic process.

Second, each pair of adjacent bits is exchanged (e.g. 01 to 10, 10 to 01, 00 and 11 unaffected) at a mean rate R, thus idealizing turbulent advection with eddy diffusivity RL^2. (Note that bits execute simple random walks with event rate $2R$.) Like laminar burning, this process is random in time, namely a Poisson process with mean event rate R for each bit pair. Model dynamics are

governed by one non-dimensional parameter, $\gamma = R/B$, which can be viewed as an idealization of the quantity u'/S that governs 3D turbulent combustion, where u' is the root-mean-square turbulent velocity fluctuation and S is the laminar flame speed. $1/B$ times the mean rate of 0-to-1 conversions is then the model analog of u_T/S, where u_T is the turbulent burning velocity.

For a step-function initial bit profile, this process relaxes to statistically steady propagation that captures some qualitative features of turbulent premixed combustion [34]. It has been shown that model analog of u_T is governed by the KPP velocity-selection principle in the large-γ limit [35]. To improve the physical realism of this formulation, it was extended by allowing exchanges of the positions of non-adjacent bit pairs, idealizing the effects of turbulent eddies of various sizes [36].

4.2 Linear-Eddy Model

Though bit-pair exchange over a range of bit separations reflects the range of eddy motions in turbulence, it does not reflect the coherence of eddy motions, meaning that a large eddy displaces a larger volume of fluid in a given direction than does a small eddy. Accordingly, an exchange process denoted block inversion was introduced, involving the reversal of the order of bits j through $j + l - 1$ to represent a size-l eddy [37]. This change was necessitated by the application of the 1D approach to diffusive scalar mixing rather than flame propagation; bit-pair exchange gives far too rapid length-scale reduction in this context. This artifact occurs also for flame propagation, but is less severe in that context because u_T is more sensitive to the distance and frequency of the largest bit displacements than to the amount of fluid transported.

Block inversion introduces scalar discontinuities at eddy endpoints. From a spectral viewpoint, this corresponds to transfer of scalar fluctuations from finite wave-number k to $k = \infty$, violating the spectral locality of length-scale reduction that is a hallmark of the inertial-range turbulent cascade [11].

To remedy this artifact, the scalar-mixing formulation, denoted the 'linear-eddy model' (LEM), was improved by introducing a new exchange process, termed the triplet map [38]. This is not a pair exchange, but rather, a permutation of cell indices j through $j + l - 1$. Taking the map range l to be a multiple of 3, the triplet map, illustrated in Fig. 1, permutes the cell indices into the new order $j,\ j+3,\ j+6,\ \ldots\ ,\ j+l-3,\ j+l-2,\ j+l-5,\ j+l-8,\ \ldots\ ,\ j+4,\ j+1,\ j+2,\ j+5,\ j+8,\ \ldots\ ,\ j+l-4,\ j+l-1$. This operation reduces the separation of any pair of cells by no more than a factor of three, thus satisfying the scale locality of length-scale reduction. It is the simplest of a family of permutations that preserve scale locality, and is optimal in that no other member of the family enforces a smaller bound B (Sect. 3.2) on the maximum scale-reduction factor. Because it is a permutation of equal-sized cells, the triplet map is measure preserving in the sense defined in Sect. 3.2.

LEM is parameterized by a Péclet number Pe, which is the eddy diffusivity associated with transport by the triplet-map sequence divided by the

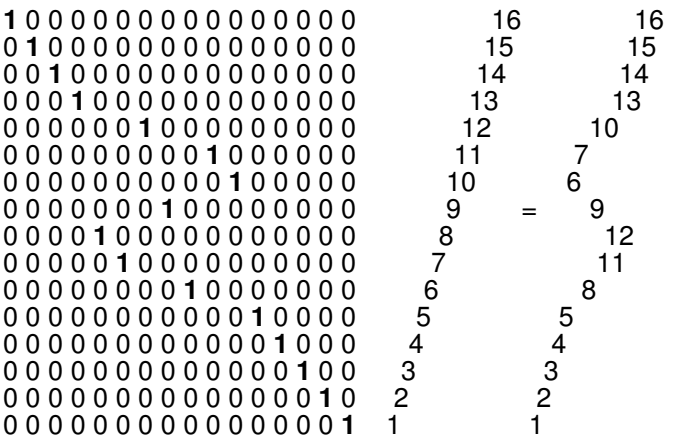

Fig. 1. Application of a triplet map, with $l = 9$, to a 16-element column vector with vertically increasing cell indices. For clarity, unity matrix elements are boldface and cells are shifted horizontally in proportion to their index values. The shifts are intended to suggest the 1D profile of the mapped variable.

molecular diffusivity. On this basis, LEM has been used to study the dependencies of turbulent mixing and reaction processes on Pe and on the initial and boundary conditions imposed on one or more scalar profiles that evolve on the 1D domain [31],[39]–[44].

4.3 One-Dimensional Turbulence

LEM simulates mixing induced by parametrically specified turbulent advection. To obtain a model that, instead, predicts turbulent flow evolution, profiles of one or more velocity components were introduced on the 1D domain, and the random selection of individual eddies (here parameterized by j, l, and time of eddy occurrence) was generalized [30]. In LEM, the eddy rate is a prescribed function of l, reflecting the known inertial-range frequency-vs.-wavenumber scaling [11], and also depends on j if the flow is spatially inhomogeneous. In the predictive flow model, denoted 'one-dimensional turbulence' (ODT), the sampling rate for each eddy (parameterized by j and l) is a function of the instantaneous flow state, based on turbulence production and dissipation mechanisms that are conventionally used to estimate eddy time scales [45]. A key distinction here is that conventional estimation based on mixing-length phenomenology is typically applied to quantities subject to some form of averaging or filtering, but in ODT, mixing-length phenomenology is applied to instantaneous property profiles that are not subject to averaging or filtering.

In ODT, the key molecular process that evolves concurrently with eddy events (i.e., the analog of laminar flame propagation in premixed combustion

and molecular diffusivity in LEM) is molecular viscosity, as prescribed by the viscous-transport term of the momentum equation. The corresponding non-dimensional parameter that governs constant-property flow evolution in ODT is a Reynolds number. In ODT, as in 3D flow simulation, the nominal Reynolds number is defined in terms of domain geometry and flow initial and boundary conditions, but the turbulent Reynolds number, defined in terms of u', the mean energy dissipation rate, and the kinematic viscosity, is an outcome of simulated flow evolution rather than an input.

Velocity profiles in incompressible ODT do not advect fluid (see Sect. 5.4 for discussion of compressible ODT), but they influence triplet-map advection through their role in determining eddy-sampling rates. In this sense they are auxiliary variables, but in addition, they are the flow observables. The tight two-way coupling between velocity-profile evolution and eddies (triplet maps advect velocity profiles) maintains overall consistency of velocity statistics and map-induced transport.

Buoyancy effects have been incorporated into ODT, and buoyant stratified flows have been studied extensively [30],[45]–[50]. In fact, buoyancy alone (velocity profiles omitted) is a sufficient input to eddy rate determination to provide a reasonable representation of some flows of interest (including the flow considered in Sect. 7.1), motivating a simplification of ODT that is termed 'density-profile evolution' (DPE) [30, 46]. ODT has also been used to study free shear flow [51]–[53], confined flow (Sect. 7.2), and combustion [54]–[56].

4.4 Higher-Dimensional Map-Based Methods

The triplet map generalizes straightforwardly to higher spatial dimensions. This generalization is found to be useful both theoretically and computationally [29]. The relaxation of advective time-stepping constraints, and the option of a mesh-free Lagrangian algorithm (based on the spatial continuum definition of the triplet map, see Sect. 5), offer substantial computational advantages even in 3D.

In higher dimensions, it is possible to define a deterministic map-based advection protocol that is a useful representation of turbulence in some contexts. One such formulation, 'deterministic turbulent mixing' (DTM), has been used to study flame-front geometry in turbulent premixed combustion [57].

5 ODT Formulation of Substructure Advancement

5.1 Boussinesq Formulation

To date, compressible gas dynamics has not been incorporated into ODT. The existing formulation that has the features closest to those needed in a compressible formulation is one that is based on the general variable-density conservation equations (i.e., not specialized to small density fluctuations) [53].

This formulation involves mathematical intricacy that obscures the underlying modeling concepts, and a compressible formulation will be even more obscure in this regard. Therefore the formulation outlined here is based on the Boussinesq approximation, in which density variations are deemed negligible except in the gravitational forcing term. Gravity is included here both to illustrate the treatment of a dynamically active scalar property (here, density) and because the initial target application of the proposed ODTLES formulation is a buoyancy-driven flow. This formulation is roughly analogous to the ODT formulation in [45].

A mathematical statement of this illustrative formulation is presented. In Sect. 4.2, a spatially discrete definition of the triplet map was given. Henceforth, space and time variables are continuous unless stated otherwise, and the triplet map is defined on the spatial continuum.

The ODT formulation utilized here simulates the time evolution of velocity components u, v, and w and density ρ defined on a 1D domain representing the vertical (z) coordinate. This evolution involves two processes: (1) a sequence of eddy events, which are instantaneous transformations that represent turbulent stirring, and (2) intervening time advancement of conventional form. Each eddy event may be interpreted as the model analog of an individual turbulent eddy. The location, length scale, and frequency of eddy events are governed by a stochastic process.

During the time interval between each eddy event and its successor, the time evolution of property profiles is governed by the equations

$$\left(\partial_t - \nu\partial_z^2\right) u(z,t) = 0 \tag{2}$$

$$\left(\partial_t - \nu\partial_z^2\right) v(z,t) = 0 \tag{3}$$

$$\left(\partial_t - \nu\partial_z^2\right) w(z,t) = 0 \tag{4}$$

$$\left(\partial_t - \gamma\partial_z^2\right) \rho(z,t) = 0. \tag{5}$$

Here ν is viscosity and γ is diffusivity of the scalar, temperature, that controls the density. For simulation of Rayleigh convection, discussed in Sect. 7.1, these equations are solved on a vertical domain $[0, H]$, where H is the height of the convection cell. Boundary conditions applied to the velocity at $z = 0$ and H are $u = v = w = 0$. Density boundary conditions are $\rho(0,t) = \rho_1$ and $\rho(H,t) = \rho_2$, where $\rho_2 > \rho_1$ to enforce unstable stratification, which drives the flow.

Each eddy event consists of two mathematical operations. One is a triplet map representing the fluid displacements associated with a notional turbulent eddy. The other is a modification of the velocity profiles in order to implement pressure-induced energy redistribution among velocity components and net kinetic-energy gain or loss due to equal-and-opposite changes of the gravitational potential energy. These operations are represented symbolically as

$$\begin{array}{lll} \rho(z) & \rightarrow & \rho(M(z)) \\ u(z) & \rightarrow & u(M(z)) + c_u K(z) \\ v(z) & \rightarrow & v(M(z)) + c_v K(z) \\ w(z) & \rightarrow & w(M(z)) + c_w K(z). \end{array} \tag{6}$$

According to this prescription, fluid at location $M(z)$ is moved to location z by the mapping operation, thus defining the map in terms of its inverse $M(z)$. This mapping is applied to all fluid properties. The additive term $c_s K(z)$, where $s = u$, v, or w, affects only the velocity components. It implements the aforementioned kinetic-energy changes. Potential-energy change is inherent in the mapping-induced vertical redistribution of the ρ profile; see (10).

In the spatial continuum, the triplet map is defined as

$$M(z) \equiv z_0 + \begin{cases} 3(z - z_0) & \text{if } z_0 \le z \le z_0 + \frac{1}{3}l, \\ 2l - 3(z - z_0) & \text{if } z_0 + \frac{1}{3}l \le z \le z_0 + \frac{2}{3}l, \\ 3(z - z_0) - 2l & \text{if } z_0 + \frac{2}{3}l \le z \le z_0 + l, \\ z - z_0 & \text{otherwise.} \end{cases} \tag{7}$$

This mapping takes a line segment $[z_0, z_0+l]$, shrinks it to a third of its original length, and then places three copies on the original domain. The middle copy is reversed, which maintains the continuity of advected fields and introduces the rotational folding effect of turbulent eddy motion. Property fields outside the size-l segment are unaffected.

The parameters z_0 and l are the continuum analogs of the integer quantities j and l in the discrete definition of the triplet map in Sect. 4.2. Here, z_0 specifies the location, and l the size, of the eddy event.

In (6), K is a kernel function that is defined as $K(z) = z - M(z)$, i.e., its value is equal to the distance the local fluid element is displaced. It is non-zero only within the eddy interval, and it integrates to zero so that the process does not change the total (z-integrated) momentum of individual velocity components. It provides a mechanism for energy redistribution among velocity components, enabling the model to simulate the tendency of turbulent eddies to drive the flow toward isotropy, constrained by the requirement of total (kinetic plus potential) energy conservation during the eddy event (which is non-dissipative).

To quantify these features of eddy energetics, and thereby specify the coefficients c_s in (6), it is convenient to introduce the quantities

$$s_K \equiv \frac{1}{l^2} \int s(M(z)) K(z)\, dz, \tag{8}$$

where $s = u$, v, w, or ρ. Substitution of the definition of $K(z)$ into (8) yields

$$s_K = \frac{1}{l^2} \int [z s(M(z)) - M(z) s(M(z))]\, dz = \frac{1}{l^2} \int [s(M(z)) - s(z)] z\, dz. \tag{9}$$

Because $M(z)$ is a measure-preserving map of the z domain onto itself, the domain integral of any function of $M(z)$ is equal to the domain integral of the

same function with argument z. This allows the substitutions of z for $M(z)$ that yield the final result in (9). For $s = \rho$, this expression is proportional to the potential-energy change induced by the triplet map. The energy change Δ caused by an eddy event can then be expressed as

$$\Delta = \rho_0 l^2 (c_u u_K + c_v v_K + c_w w_K) + \frac{2}{27} \rho_0 l^3 (c_u^2 + c_v^2 + c_w^2) + g l^2 \rho_K, \qquad (10)$$

where a reference density ρ_0 (defined here as mass per unit height, based on a nominal column cross-section) is introduced (i.e., the standard Boussinesq prescription), as well as the gravitational acceleration g.

The representation of both the potential and kinetic energy contributions in (10) using (8) is a consequence of the definition chosen for K. Based on this definition, another equivalent form of (8),

$$s_K \equiv \frac{4}{9l^2} \int_{z_0}^{z_0+l} s(z)[l - 2(z - z_0)]\, dz, \qquad (11)$$

which is useful for numerical implementation, is readily obtained.

Overall energy conservation requires $\Delta = 0$. Two additional conditions are required to specify the coefficients c_s. These are based on a representation of the tendency for eddies to induce isotropy. For this purpose, it is noted that there is a maximum amount $Q_s = \frac{27}{8} \rho_0 l s_K^2$ of kinetic energy that can be extracted from a given velocity component s during an eddy event [52]. (The amount of energy actually extracted or deposited depends on c_s.) Q_s is thus the 'available energy' in component s prior to event implementation. The tendency toward isotropy is introduced by requiring the available energies of the three velocity components to be equal upon completion of the eddy event. This provides the additional needed conditions and yields the following expression determining c_s:

$$c_s = \frac{27}{4l} \left[-s_K \pm \sqrt{\frac{1}{3} \left(u_K^2 + v_K^2 + w_K^2 - \frac{8gl}{27} \frac{\rho_K}{\rho_0} \right)} \right]. \qquad (12)$$

The physical criterion that resolves the sign ambiguity is explained in [52]. Note that the last term in (12) is the square root of a quantity proportional to the net available energy $Q_u + Q_v + Q_w - P$, where the quantities Q_s are the component available energies prior to event implementation and P is the gravitational potential energy change caused by triplet-mapping of the ρ profile, requiring equal-and-opposite change of available energy during eddy implementation, as enforced by the condition $\Delta = 0$. If P is positive (stable stratification) and larger than the available energy, then the eddy is energetically prohibited. In this case, the argument of the square root in (12) is negative and the eddy event is not implemented (see below).

Although the formulation of an individual eddy event incorporates several important features of turbulent eddies, the key to the overall performance of

the model is the procedure for determining the sequence of eddy events during a simulated flow realization. The expected number of eddies occurring during a time interval dt, whose parameter values are within dz of z_0 and within dl of l, is denoted the 'eddy rate distribution' $\lambda(z_0, l; t)\, dz_0\, dl\, dt$, which has units of $(\text{length}^2 \times \text{time})^{-1}$. Eddies are randomly sampled from this distribution. Mathematically, this generates a marked Poisson process [58] whose mean rate as a function of the 'mark' (parameter) values z_0 and l varies with time. The physical content of the eddy selection process is embodied in the expression for λ that is adopted,

$$\lambda = \frac{C\nu}{l^4}\sqrt{\left(\frac{u_K l}{\nu}\right)^2 + \left(\frac{v_K l}{\nu}\right)^2 + \left(\frac{w_K l}{\nu}\right)^2 - \frac{8gl^3}{27\nu^2}\frac{\rho_K}{\rho_0} - Z}. \qquad (13)$$

This expression involves two free parameters, C and Z, whose roles are explained in Sect. 6.2. λ is set equal to zero if the argument of the square root is negative, indicating an energetically prohibited event; see the discussion of (12).

For $Z = 0$, the argument of the square root is a scaled form of the net available energy. Thus, for given z_0 and l, (13) with $Z = 0$ is simply the dimensionally consistent relation between the net available energy and the length and time scales of eddy motion, where the associated time scale is the inverse of the (appropriately normalized) eddy rate λ. Thus, (13) may be viewed as a representation of mixing-length phenomenology within the ODT framework. This phenomenology is the basis of many turbulence modeling approaches. In particular, it is central to LES closures based on eddy viscosity, hence the analogy between conventional LES and the proposed ODTLES methodology (Sect. 3.4). However, the present approach, which does not involve averaging, differs from the typical use of mixing-length concepts to close averaged equations in several respects:

1. Rather than assigning a unique l value at each spatial location, ODT allows eddies of all sizes throughout the spatial domain, with their relative frequencies of occurrence at different locations specified by (13).
2. Quantities on the right-hand side of (13) depend on the instantaneous flow state rather than an average state, so eddy occurrences are responsive to unsteadiness resulting from transient forcing or statistical fluctuations inherent in the eddy-sampling process.
3. Eddy occurrences thus depend on the effects of prior eddies and affect future eddy occurrences. These dependencies induce spatio-temporal correlations among eddy events, leading to a physically based representation of turbulence intermittency.

These attributes of ODT are the basis of its detailed representation of turbulent cascade dynamics coupled to boundary conditions, shear and buoyant forcing, etc. In particular, the stochastic variability of simulated ODT realizations arises from a physically based representation of turbulent eddy statistics, and thus enables a conceptually sound and mathematically consistent

assessment of the effects of stochastic variability on the variability of, and correlations among, output statistics.

If two of the three velocity components are removed from the model, (13) reduces to the eddy rate distribution used in [48]. If the buoyancy term is omitted, (13) resembles the expression for λ that appears in [52], except that here, λ is based on the total available energy (including contributions from all three velocity components) rather than the available energy associated with vertical motion. Use of the total available energy is advantageous here because it gives the correct critical Richardson number, $Ri_c = \frac{1}{4}$ [59], for the onset of instability (in the present context, eddy events). Another distinction from [52] is that the procedure that was used previously to suppress occasional unphysically large eddy events is omitted here. For ODTLES implementation, a bound on eddy sizes follows from consideration, in Sect. 6.2, of the complementary roles of steps 1 and 2 of the advancement cycle.

5.2 Numerical Implementation of Eddy Sampling

The unsteadiness of the rate distribution λ suggests the need to reconstruct this distribution continuously as the flow state evolves. This prohibitively costly procedure is avoided by an application of the rejection method [60], involving eddy sampling based on an arbitrary sampling distribution that is designed to over-sample all eddies. True rates are computed only for sampled eddies, and are used to determine eddy acceptance probabilities. The resulting procedure adequately approximates the desired sampling from λ [30], and is exact in the limit of infinite over-sampling. The choice of the arbitrary sampling distribution affects the efficiency of the sampling procedure, but not the statistics of the eddies that are selected for implementation.

This implies modification of the split-operator cycling during 1D advancement that is outlined at the end of Sect. 3.2. Denoting the arbitrary joint PDF used to sample z_0 and l values as $h(z_0, l)$, and choosing a sufficiently small eddy-sampling time-step Δt_s, the advancement cycle during step 1 of the overall advancement (Sect. 3.3) is

1. Advance the concurrent processes such as viscous transport (Sect. 3.3) for a time interval Δt_s.
2. Sample z_0 and l values from $h(z_0, l)$.
3. For these values, compute $\lambda(z_0, l)$ based on the current flow state.
4. Compute the ratio P of the rate $\lambda(z_0, l)$ of occurrence of an eddy with these z_0 and l values as given by the model to the rate $h(z_0, l)/\Delta t_s$ resulting from the sampling procedure.
5. Implement the selected eddy with probability P based on a Bernoulli trial, i.e., implement the eddy if $P = \lambda(z_0, l)\Delta t_s / h(z_0, l)$ is larger than a random variable sampled from the uniform distribution over $[0, 1]$).

Δt_s must be assigned a value small enough so that P never exceeds unity. For numerical accuracy, $P \ll 1$ should be obeyed with at most rare exceptions.

For an evolving flow, it is efficient to adjust Δt_s during advancement in order to direct the P values toward a target range, typically of order 0.01.

5.3 Planar Free Shear Flows

The ODT representation of a time-developing Kelvin–Helmholtz instability, illustrated in Fig. 2, indicates some of the flow features captured by the model. This illustration is based on the ODT formulation of [52], which includes the large-eddy suppression procedure that is needed for stand-alone ODT simulation of unbounded flows (Sect. 5.1).

The rendering shows that the width of the active mixing zone grows primarily by the relatively infrequent occurrence of a large event extending beyond the current range of the mixing zone, with some additional contribution by the more numerous small events. This process is consistent with the dominant role of large engulfing motions and the secondary role of small-scale nibbling in turbulent entraining flows under neutral buoyancy conditions. (The effect of density stratification on the ODT representation of turbulent entrainment has been investigated [30, 53].)

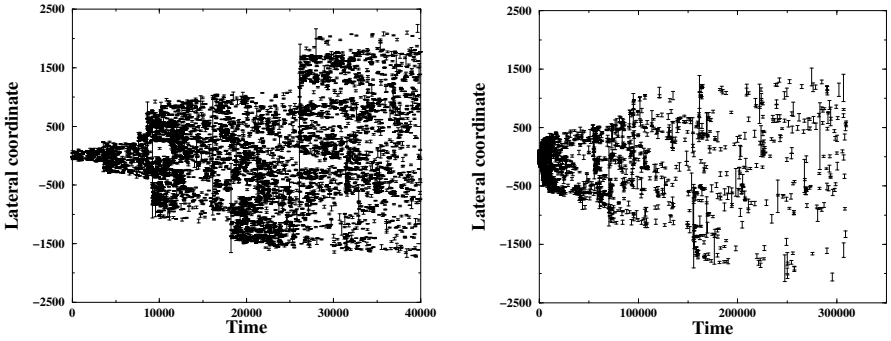

Fig. 2. Graphical representation of the sequence of eddy events during a simulated ODT realization of a time-developing Kelvin–Helmholtz instability (left panel) and a time-developing planar wake (right panel) [52]. The Kelvin–Helmholtz and wake simulations are initialized using step-function and top-hat initial velocity profiles, respectively. The space and time units in this illustration are arbitrary. In the plots, each eddy is represented by an error bar whose vertical span corresponds to the eddy range $[z_0, z_0 + l]$, and whose horizontal location corresponds to the time of eddy occurrence.

Bunching of events, especially after the occurrence of a large event, reflects the interactions between the eddy events and the evolving velocity profile that induce the model analog of the turbulent cascade. Each eddy event compresses

and folds the velocity profile within the range of the event. This increases the local shear that contributes to mechanical turbulence production in the relation (13) governing the frequency of subsequent events within that range. (In stratified flows, the buoyant production is also affected.) A feedback process is thus induced that promotes the occurrence of successively smaller events. Eventually, velocity fluctuation length scales are reduced sufficiently so that damping of the fluctuations by concurrent viscous transport dominates the production of fluctuations by eddy events. Viscous damping thus terminates the local burst of eddy activity.

A planar wake simulation is also shown in Fig. 2. In the Kelvin–Helmholtz simulation, vigorous turbulence, indicated by the number and size range of eddies as the flow evolves, is sustained by the shear imposed on the flow by the free-stream conditions (far-field velocity difference). The wake, however, evolves in a uniform background. As the initial velocity perturbation is dispersed by eddies and dissipated by concurrent viscous evolution, the turbulence intensity decreases, affecting the eddy frequency and size range and slowing the growth of the turbulent zone. These qualitative impressions are supported by the quantitative consistency of ODT simulation statistics with the known similarity scalings for these flows [52].

5.4 Proposed Compressible Formulation

The main modifications of the Boussinesq ODT formulation that are required in order to incorporate compressible gas dynamics are:

1. During 1D advancement, the w velocity now advects all properties, so introduce a $w\frac{d}{dz}$ term on the left-hand side of (2)–(4) and in the additional evolution equations mentioned below (item 4).
2. Adopt the general variable-density formulation of [53], which generalizes the momentum equations (2)–(4) and the energy-redistribution step during eddy implementation.
3. In the w equation, introduce a pressure-gradient (dp/dz) term.
4. Introduce 1D continuity and energy equations, and an equation of state (e.g., ideal gas) that determines the pressure locally (in each wafer) from density, temperature, and composition (for multi-species mixtures).
5. Generalize the potential-energy contribution in (13) to reflect the equivalence of the gravitational body force and dw/dt acceleration.
6. Generalize the viscous stress terms in (2)–(4) to compressible form, introducing (manageable) complications that are not elaborated here.

This scheme introduces acoustic time scales, which are very short relative to other time scales at low Ma. As in other low-Ma compressible simulations, a pseudo-compressible scheme based on an artificially low sound speed [1] can improve the efficiency of this formulation at low Ma.

A poorly understood feature of compressible turbulence is the coupling of acoustic and vortical motions. Because w is an advecting velocity rather than

an auxiliary variable in the proposed compressible formulation, the triplet map introduces such a coupling. For example, if the property profile in Fig. 1 is taken to be the w profile, then in this instance the map, representing vortical motion, converts a pure expansion into an alternating expansion-compression-expansion, i.e., an acoustic source. Given the limited state of understanding of vortical-acoustic coupling in compressible turbulence, it is difficult to ascertain whether this is a good representation of this coupling.

This question is best addressed by implementing the proposed formulation and evaluating its predictive capabilities. Unlike incompressible ODT (Sect. 5.1), this compressible formulation is not intended for use as a stand-alone model. Its incorporation into 3D ODTLES is now considered.

6 ODTLES

6.1 Features

For implementation within ODTLES, an important feature of the formulation of Sect. 5.4 is the distinguished role of w in the z solution (and likewise of u and v in the x and y solutions, respctively). Here it is convenient to introduce the alternate notation $v_{j,k}$ denoting velocity component j in solution k. The component $v_{i,i}$ now advects properties in solution i, but for $j \neq i$, components $v_{j,i}$ are auxiliary variables in solution i, as in Sect. 5.1. In addition to their usual role in determining the eddy sampling rate, these components, like all other flow properties, are fluxed through CV faces, thus prescribing inter-domain transfers of these velocity components in the $j \neq i$ flow solutions (step 2 of the advancement cycle; see Sect. 3.3). In this manner they influence the evolution of the advecting components $v_{j,j}$ in the $j \neq i$ solutions.

This highlights the multi-faceted relationships among the three velocity components, the three flow solutions and the two steps of the advancement cycle. A related consideration is the manner in which the simulated evolution communicates pressure effects in 3D. If the pressure is locally high in one of the solutions, it is likely to be high is the same vicinity in the other solutions because they are all subject to the same fluxes at CV face locations (enforced by advancement step 2). Then step-1 (1D compressible) advancement in each solution will generate flow directed away from this vicinity in one coordinate direction. Step 2 will then communicate these outward-directed flows among the solutions so as to yield an approximate representation of radial outflow from the high-pressure region in all the solutions.

Step 2 transfers properties over a distance unity, rather than the 1D resolution scale $1/m$, using first differences. This is a diffusive representation of fluxes that are primarily advective, and therefore induces numerical dissipation of kinetic energy. Conservation of total energy, which is obeyed exactly, implies conversion of the lost kinetic energy into heat. For conventional eddy-diffusivity closure, incorporation of a subgrid energy evolution equation can

recast this dissipation as conversion of mesh-resolved kinetic energy into subgrid kinetic energy, with subsequent conversion to heat by viscous dissipation. The analogous mechanism in ODT is the use of the kernel operation to deposit the numerically dissipated energy into the velocity fields. Using the method of [53], this can be done in conformance with momentum conservation for variable-density flows. To distinguish numerically dissipated energy from true viscous dissipation, separate accounting of advective and viscous fluxes across CV faces is needed. This can be done by straightforward generalization of the procedure used in [52] to variable-density flow.

Because step 2 involves diffusive representation of advective transport, it is subject to some of the same limitations as parameterizations in which this the representation of advective transport below 3D mesh-resolved scales is solely diffusive. Nevertheless, owing to the 1D sub-cycling during step 1, salient characteristics of the small scale flow structure are preserved, as has been demonstrated using the formulation described in Sect. 6.3 [20]. Splicing is a different method for implementing step-2 property transfers that is not diffusive in character, but is subject to other limitations, as noted in Sect. 2.5.

Because step 2 of the advancement cycle applies fluxes to a given flow solution that are interpolants of fluxes in a different flow solution, it is mathematically possible to violate realizability. Namely, it is possible to flux more of a non-negative quantity such as mass out of a wafer than it contains. This establishes a CFL-type constraint on the time step Δt. The allowed magnitude of Δt is of the same order for ODT closure as for eddy-diffusivity closure in which there is no spatial refinement below the CV scale, though for ODT the constraint is slightly more restrictive due to stochastic variability. Use of a small value of Δt incurs no significant cost penalty because the 1D sub-cycling using smaller time steps is the most costly part of the computation.

As noted in Sect. 3.3, Gauss' theorem constrains the evolution of the three distinct solutions. For each flow solution, it implies that the change of the CV integral of a conserved property during one advancement cycle is equal to the sum of the transfers of those properties through CV faces. The flux across each face is operationally defined as the corresponding face transfer divided by the time step Δt. (Recall that the face area is unity in scaled units.) This identity motivates a definition of mesh-scale output statistics that conserves the property exactly. Consider total CV mass, denoted $\bar{\rho}$ because the scaled volume is unity. Gauss's theorem implies that the quantities $\bar{\rho}$ and the face fluxes of mass, i.e. momenta $\langle \rho v \rangle_{\rm face}$ (where v is the face-normal velocity), form a conservative set of output variables. An additional assumption or definition is needed to define the mesh-scale face velocity V. A natural choice is $\langle \rho v \rangle_{\rm face} \equiv \langle \rho \rangle V$, where $\langle \rho \rangle$ is an interpolant of the $\bar{\rho}$ array evaluated at the face center at the midpoint $\Delta t/2$ of the advancement cycle (corresponding to the midpoint of the time integration that determines mass transfers across faces).

An output protocol of this sort is needed because the 3D conservation laws are applicable only to CVs and only with reference to state changes from

the beginning to the end of the advancement cycle. Analogous considerations arise in conventional advancement schemes.

Discrete and continuum definitions of the triplet map are provided in Sects. 4.2 and 5.1 respectively, where the former is applicable in the Eulerian uniform-mesh (Sect. 3.1) implementation described thus far. In ongoing work, an alternative Lagrangian-mesh ODT implementation has been developed in which wafer faces are advected by the w velocity (if the flow is compressible) and by triplet maps. Here, the continuum map definition is used, resulting in tripling of the number of wafer faces within the mapped interval. A mesh-management scheme is used to suppress the excessive proliferation of wafers. This formulation will be particularly advantageous for wall-bounded flows in which high spatial resolution is needed only in near-wall regions, as in the applications discussed in Sect. 7.

6.2 Parameter Assignment

The model parameters C and Z are introduced in the formulation of eddy sampling in Sect. 5.1. C scales the eddy event rate, and hence the simulated turbulence intensity, for a given flow configuration. The role of Z is to impose a threshold eddy Reynolds number that must be exceeded to allow eddy occurrence [45]. In near-wall flow, the transition from the viscous layer to the buffer layer is sensitive to this threshold and hence to Z [61]. For $Z > 0$, eddies are suppressed entirely when local values of the eddy Reynolds number are sufficiently small. The circumstances under which this occurs in ODTLES are considered. This question is closely tied to the upper bound on the range of allowed eddy sizes l.

As noted in Sect. 6.1, the 3D character of the flow is captured above the CV scale by step 2 of the advancement cycle. Therefore it would be redundant to allow l values greatly exceeding unity. Likewise, the bound on l should not be much less than unity, because this would omit representation of eddies larger than the bound but smaller than unity. The signature of either of these artifacts would be apparent in the 1D energy spectrum, which can be extracted from ODT simulations [20, 30, 33]. Examination of energy spectra from simulations of representative flows therefore allows empirical determination of a bound on l.

As noted, the bound will be of order unity. Therefore the largest Reynolds number of a 1D eddy event that will occur is of the order of the Reynolds number of the largest eddy that is not resolved at the CV scale. If the mesh is increasingly refined (decreasing CV size in physical units) for a given flow configuration, then the Reynolds number of the largest unresolved eddy decreases until it is below the threshold value corresponding to the assigned value of Z. At this mesh refinement, eddies are entirely suppressed during 1D sub-cycling, so no fine structure is generated and additional 1D refinement below the CV scale (i.e., $m \gg 1$) becomes superfluous. At this point, the role of physical modeling is eliminated and the ODTLES simulation reduces

to DNS. This and the considerations of Sect. 3.4 highlight the nature of the assumptions and approximations on which ODTLES is based.

6.3 Comparison Case: Incompressible Formulation

An incompressible analog of the formulation of Sect. 6.1 has been developed and applied to homogeneous decaying turbulence [20]. The main differences between the two formulations are summarized.

Because the incompressible formulation precludes dilatational flow, continuity must be enforced on a time-accurate basis. Therefore a two-step advancement cycle similar to that described in Sect. 3.3 is implemented at subcycling (order Δt_s) time intervals rather than the much larger time interval Δt of the complete advancement cycle. Each 1D domain evolves the two velocity components $v_{j,k}$ for $j \neq k$. The $j = k$ component that advects fluid in the compressible formulation is omitted. Instead, fluid is advected along the 1D domain by a separately defined 'advecting velocity' that is determined by continuity (here, the solenoidal condition), based on 'fluxing velocities' that govern inter-domain transfers (the analog of step 2 in Sect. 3.3). The fluxing velocities are moving averages, in time, of the velocity components evolved on the 1D domain. (This is an incomplete description because it omits consideration of the staggered mesh on which the simulation is implemented, and its algorithmic implications.)

Once per overall advancement cycle (which in fact is a sub-cycle within a fractional-step scheme), a pressure projection is performed to enforce continuity of the mesh-scale filtered velocity field. The resulting velocity corrections are passed down to the 1D level using an adjustment scheme involving a momentum-conserving interpolant of the mesh-scale corrections. The interpolant is slightly dissipative, but this can be corrected where it degrades the flow solution using the kernel operation, as in Sect. 6.1.

It seems likely that this and the compressible formulation will exhibit comparable performance for flow regimes to which both can be applied, but this remains to be demonstrated. Computational costs are also likely to be comparable. Other perspectives on ODT-based 3D simulation of incompressible turbulent flow are provided in [32] and [62].

7 Illustrative ODT Applications

7.1 Rayleigh Convection

Rayleigh convection is a suitable initial application for compressible ODTLES. Here, previously reported results for this flow [50] obtained using the Boussinesq ODT formulation of Sect. 5.1 are summarized in order to illustrate the performance of ODT and the additional predictive capability that might be provided by compressible ODTLES.

The ODT formulation used to simulate Rayleigh convection was simpler than that of Sect. 5.1 in that one instead of three velocity components was evolved. An even simpler ODT-type formulation was previously used to simulate this flow [30]. Termed 'density profile evolution' (DPE), it evolves only density or a density surrogate (temperature), but no velocity components. Equation (13) indicates that in a gravitationally unstable state, gravitational potential energy, in the absence of fluid motion, is sufficient to generate eddy motion, consistent with the physical occurrence of spontaneous onset of motion under such conditions (e.g., the Rayleigh–Taylor instability, which has also been simulated using DPE [30]). Other buoyant-stratified-flow applications of both DPE [46] and one-component ODT [47, 48, 49] have been reported.

The ODT representation of Rayleigh convection corresponds to the ideal configuration of horizontally homogeneous flow between horizontal plates of infinite extent, but computed results are compared to measurements in convection cells that are necessarily laterally bounded. The dimensional parameters governing this flow, which are plate separation, buoyant forcing, viscosity ν, and thermal conductivity κ, are grouped into two non-dimensional parameters, the Rayleigh number Ra, which quantifies the strength of the gravitational instability, and the Prandtl number $\mathrm{Pr} = \nu/\kappa$, a fluid property that controls the relative thicknesses of the near-wall viscous and thermal layers. At high Ra, the thin near-wall layers strongly influence flow dynamics, as demonstrated by the significant observed Pr dependence of flow structure [63]. ODT is an efficient method for resolving these thin layers.

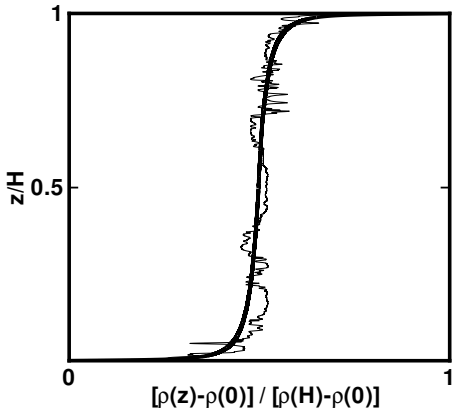

Fig. 3. Instantaneous (thin line) and time averaged (thick line) vertical profiles of normalized density from an ODT simulation of Rayleigh convection for $\mathrm{Ra} = 1.4 \times 10^9$ and $\mathrm{Pr} = 0.7$.

In Fig. 2, an instantaneous density profile from an ODT simulation of Rayleigh convection highlights the analogies between the model and physical processes in the flow. Large localized deviations from the time averaged profile are the signatures of map-induced displacements of near-wall fluid into the bulk flow region. Though these displacements do not capture the persistence in time of buoyant plumes, they emulate the mechanism of entrainment of near-wall fluid into the bulk flow. Smaller eddy events sub-divide and compress entrained parcels (upper region of the profile). In conjunction with molecular transport, this leads to smoothing of the fluctuations (e.g., smooth regions in the central and lower regions of the profile that deviate from the time average). Over time, these processes communicate wall forcings to the center plane, as indicated by the nonzero density gradient at the center of the profile. Using ODT, these flow mechanisms have been quantitatively characterized [50], which in turn has motivated another innovative modeling approach [64].

The behavior of greatest interest is the dependence of the turbulent enhancement of mean heat flux, denoted Nu (Nusselt number), on Ra and Pr. Adjustment of the model parameters, C and Z, yields good agreement with measured Nu values over a wide range of Ra and Pr values. Without further adjustment, ODT yields accurate predictions of center-plane fluctuations, including PDFs of velocity and temperature [50].

Comparison of near-wall simulated PDFs with measurements [65] indicates large discrepancies that may reflect the inability of ODT to capture the 'wind,' a symmetry-breaking large scale circulation [66]. Given the good performance of the model in other respects, an ODTLES formulation that incorporates 3D boundary conditions and emulates 3D large scale motions might reproduce the wind and its influence on fluctuation statistics. This will be a useful initial test of the compressible formulation, both because conventional methods cannot affordably capture the relevant small scale near-wall phenomena and because copious experimental data, exhibiting non-trivial parameter dependencies, are available.

The confinement of influential small scale phenomena to the near-wall region implies a strong preference for the Lagrangian numerical scheme, which by construction provides high resolution only where needed. It can therefore be anticipated that this application will be no more costly computationally than a previously demonstrated near-wall ODT closure for confined flows (Sect. 7.2), which was used to simulate high-Re channel flow on a single processor [61].

7.2 Channel Flow

Channel flow corresponds to the the same geometry as idealized Rayleigh convection , i.e., flow between parallel plates with no-slip boundary conditions, but the flow is forced by a pressure gradient parallel to the plates rather than gravitation normal to the plates. Like Rayleigh convection, channel flow relaxes to a statistically steady state. It is a canonical test case for conventional LES [67, 68].

To address the near-wall closure difficulties described in Sect. 2.1, an ODT-based near-wall subgrid closure for LES was implemented and applied to channel flow [61]. The closure is similar in structure to, and in fact was the precursor of, the formulation described in Sect. 6.3. In this regard, it might appear that the full-flow closure is superfluous away from the near-wall region. (As in Rayleigh convection, small scale motion and transport are disproportionately influential only in the near-wall region.) For channel flow specifically, this may be correct, but the compressible formulation with Lagrangian 1D implementation may be comparable in cost, as is expected for Rayleigh convection. Moreover, the near-wall closure involves potentially problematic parameterization in the region of transition between the ODT near-wall treatment and conventional closure in the bulk flow.

As in the application to Rayleigh convection, ODT parameters were adjusted to match a mean flow property, in this case, the mean velocity profile. Here, Z controls the height of the transition from the viscous to the buffer region. The LES with ODT subgrid closure reproduced the friction law and wall-normal profiles of velocity fluctuations with good accuracy. Stand-alone ODT yielded less accurate near-wall fluctuation statistics, indicating the need for a 3D bulk-flow representation in order to represent accurately the bulk forcing that drives near-wall fluctuations. It is anticipated (Sect. 7.1) that ODTLES may likewise capture the wind effect in Rayleigh convection, yielding comparable performance improvements relative to stand-alone ODT.

8 Discussion

High-fidelity simulation of turbulent flows and their interaction with other processes ultimately requires local (in space and time) resolution of all relevant processes. Because this is unaffordable in 3D DNS, a modeling strategy involving resolution of small scales in 1D is proposed. The drawbacks of two-way information transfer between resolved and coarse-grained treatments suggests that an all-scale 1D formulation should be adopted, with large scale 3D motion captured through suitable couplings within and among arrays of 1D domains rather than through a separate coarse-grained treatment. A proposed formulation within this 'autonomous microstructure evolution' paradigm has been outlined. The underlying 1D methodology, 'one-dimensional turbulence,' has been described, with emphasis on the gain in fidelity when a resolved 1D representation of relevant flow phenomenology is introduced.

The concept that enables the representation of turbulent fluid motion in 1D is generalization of the usual mathematical representation of advection by introducing a map-based representation. It is noted that this concept is not specific to 1D, and has potentially useful 3D applications.

Although the specific 3D turbulence simulation method outlined here has not yet been implemented or demonstrated, steps in its development that are indicative of its ultimate form and performance have been described. An

analog of this engineering-focused approach that is under development by the atmospheric science community has been noted. The potential for fruitful cross-fertilization of ideas across disciplines is plainly evident.

Acknowledgement

The author thanks R. Ecke for sharing unpublished results, and R. Schmidt and S. Wunsch for efforts and insights that were largely responsible for the progress reported here. This research was supported by the U.S. Department of Energy, Office of Basic Energy Sciences, Division of Chemical Sciences, Geosciences, and Biosciences. Sandia National Laboratories is a multi-program laboratory operated by Sandia Corporation, a Lockheed Martin Company, for the United States Department of Energy under contract DE-AC04-94-AL85000.

References

1. E.F. Toro: *Riemann Solvers and Numerical Methods for Fluid Dynamics*, 2nd edn (Springer, Berlin Heidelberg New York 1999)
2. B.J. Alder, A.J.C. Ladd: Simulation by molecular dynamics. In: *Encyclopedia of Applied Physics*, vol 18, ed by G.L. Trigg (VCH, New York 1997) p 281
3. G.R. Liu, M.B. Liu: *Smoothed Particle Hydrodynamics: A Meshfree Particle Method* (World Scientific, Singapore 2003).
4. E.G. Flekkøy, P.V. Coveney, G. De Fabritiis: Phys. Rev. E **62**, 2140 (2000)
5. S. Succi: *The Lattice Boltzmann Equation for Fluid Dynamics and Beyond* (Oxford Univ. Press, Oxford 2001)
6. S.B. Pope: Prog. Energy Combust. Sci. **11**, 119 (1985)
7. A. Leonard: J. Comput. Phys. **37**, 289 (1980)
8. A. Leonard: Annu. Rev. Fluid Mech. **17**, 523 (1985)
9. G.S. Winckelmans, A. Leonard: J. Comput. Phys. **109**, 247 (1993)
10. P. Sagaut: *Large Eddy Simulation for Incompressible Flows*, 3rd edn (Springer, Berlin Heidelberg New York 2006)
11. U. Frisch: *Turbulence: The Legacy of A.N. Kolmogorov* (Cambridge Univ. Press, Cambridge 1995)
12. V. Yakhot, K.R. Sreenivasan: J. Stat. Phys., in press (2006)
13. D.A. Randall, M. Khairoutdinov, A. Arakawa, W. Grabowski: Bull. Amer. Meteor. Soc. **84**, 1547 (2003)
14. S.K. Krueger: J. Atmos. Sci. **45**, 2221 (1988)
15. K.-M. Xu, S.K. Krueger: Mon. Wea. Rev. **119**, 342 (1991)
16. D.A. Randall, K.-M. Xu, R.C.J. Somerville, S.F. Iacobellis: J. Climate **9**, 1683 (1996)
17. J.-H. Jung, A. Arakawa: Mon. Wea. Rev. **133**, 649 (2005).
18. A.A. Townsend: *The Structure of Turbulent Shear Flow*, 2nd edn (Cambridge Univ. Press, Cambridge 1976)
19. N. Peters: *Turbulent Combustion* (Cambridge Univ. Press, Cambridge 2000)

20. R.C. Schmidt, R. McDermott, A.R. Kerstein: ODTLES: A model for 3D turbulent flow based on one-dimensional turbulence modeling concepts. Sandia National Laboratories Report SAND2005-0206 (2005)
21. V.K. Chakravarthy, S. Menon: Flow Turb. Combust. **65**, 133 (2000)
22. V.K. Chakravarthy, S. Menon: Combust. Sci. Tech. **162**, 175 (2001)
23. W.G. Vincenti, C.H. Kruger: *Introduction to Physical Gas Dynamics* (Krieger, Melbourne 1975)
24. X. Xu, J.S. Lee, R.H. Pletcher: J. Comput. Phys. **203**, 22 (2005)
25. G.K. Batchelor: *An Introduction to Fluid Dynamics* (Cambridge University Press, New York 1977)
26. A. Chekhlov, V. Yakhot: Phys. Rev. E **51**, R2739 (1995)
27. A. Juneja, D.P. Lathrop, K.R. Sreenivasan, G. Stolovitzky: Phys. Rev. E **49**, 5179 (1994)
28. T. Vicsek, A.-L. Barabási: J. Phys. A: Math. Gen. **24**, L845 (1991)
29. A.R. Kerstein, S.K. Krueger: unpublished (2006)
30. A.R. Kerstein: J. Fluid Mech. **392**, 277 (1999)
31. A.R. Kerstein: J. Fluid Mech. **231**, 361 (1991)
32. R.J. McDermott: Toward one-dimensional turbulence subgrid closure for large-eddy simulation. Ph.D. Thesis, University of Utah, Salt Lake City (2005)
33. R.J. McDermott, A.R. Kerstein, R.C. Schmidt: J. Turb., in press (2005)
34. A.R. Kerstein: J. Stat. Phys. **45**, 921 (1986)
35. M. Bramson, P. Calderoni, A. De Masi, P.A. Ferrari, J.L. Lebowitz, R.H. Schonmann: J. Stat. Phys. **45**, 905 (1986)
36. A.R. Kerstein: Proc. Combust. Inst. **21**, 1281 (1988)
37. A.R. Kerstein: Combust. Sci. Tech. **60**, 391 (1988)
38. A.R. Kerstein: Combust. Sci. Tech. **81**, 75 (1992)
39. A.R. Kerstein: Phys. Fluids A **3**, 1110 (1991)
40. A.R. Kerstein: J. Fluid Mech. **240**, 289 (1992)
41. P.A. McMurtry, T.C. Gansauge, A.R. Kerstein, S.K. Krueger: Phys. Fluids A **5**, 1023 (1993)
42. M.A. Cremer, P.A. McMurtry, A.R. Kerstein: Phys. Fluids **6**, 2143 (1994)
43. A.R. Kerstein, P.A. McMurtry: Phys. Rev. E **50**, 2057 (1994)
44. A.R. Kerstein, M.A. Cremer, P.A. McMurtry: Phys. Fluids **7**, 1999 (1995)
45. A.R. Kerstein, S. Wunsch: Bound. Layer Meteorol., in press (2005).
46. A.R. Kerstein: Dyn. Atmos. Oceans **30**, 25 (1999)
47. T.D. Dreeben, A.R. Kerstein: Int. J. Heat Mass Transf. **43**, 3823 (2000)
48. S. Wunsch, A.R. Kerstein: Phys. Fluids **13**, 702 (2001)
49. S. Wunsch: Phys. Fluids **15**, 1442 (2003)
50. S. Wunsch, A.R. Kerstein: J. Fluid Mech. **528**, 173 (2005)
51. A.R. Kerstein, T.D. Dreeben: Phys. Fluids **12**, 418 (2000)
52. A.R. Kerstein, Wm.T. Ashurst, S. Wunsch, V. Nilsen: J. Fluid Mech. **447**, 85 (2001)
53. Wm.T. Ashurst, A.R. Kerstein, Phys. Fluids **17**, 025107 (2005)
54. T. Echekki, A.R. Kerstein, J.-Y. Chen, T.D. Dreeben: Combust. Flame **125**, 1083 (2001)
55. J.C. Hewson, A.R. Kerstein: Combust. Theor. Model. **5**, 669 (2001)
56. J.C. Hewson A.R. Kerstein: Combust. Sci. Tech. **174**, 35 (2002)
57. J.C. Niemeyer, A.R. Kerstein: Combust. Sci. Tech. **128**, 343 (1997)
58. D.L. Snyder, M.I. Miller: *Random Point Processes in Time and Space*, 2nd edn (Springer-Verlag, New York 1991)

59. J.S. Turner: *Buoyancy Effects in Fluids*, 2nd edn (Cambridge Univ. Press, Cambridge 1979)
60. P. LEcuyer: Random number generation. In: *Handbook of Computational Statistics*, ed by J.E. Gentle, W. Haerdle, Y. Mori (Springer–Verlag, Berlin 2004) chap 2
61. R.C. Schmidt, A.R. Kerstein, S. Wunsch, V. Nilsen: J. Comput. Phys. **186**, 317 (2003)
62. A.R. Kerstein: Computer Phys. Commun. **148**, 1 (2002)
63. E.D. Siggia: Annu. Rev. Fluid Mech. **26**, 137 (1994)
64. S. Grossmann, D. Lohse: Phys. Fluids **16**, 4462 (2004)
65. R.E. Ecke: unpublished
66. K.R. Sreenivasan, A. Bershadskii, J.J. Niemela: Phys. Rev. E **65**, 056306 (2002)
67. W. Cabot, P. Moin: Flow Turb. Combust. **63**, 269 (1999)
68. U. Piomelli, E. Balaras: Annu. Rev. Fluid Mech. **34**, 349 (2002)

Index